CONF-960459--1

LA-UR- 95-3443

Title: ASSESSMENT OF DAMAGE IDENTIFICATION ALGORITHMS ON EXPERIMENTAL AND NUMERICAL BRIDGE DATA

Author(s): David V. Jauregui, Los Alamos National Laboratory, ESA-EA
Los Alamos, New Mexico

Charles R. Farrar, Los Alamos National Laboratory, ESA-EA
Los Alamos, New Mexico

Submitted to: 1996 ASCE Structures Congress
April 15 - 18, 1996
Chicago, IL

Los Alamos
NATIONAL LABORATORY

Assessment of Damage Identification Algorithms on Experimental and Numerical Bridge Data

David V. Jauregui[1], S. M. ASCE and Charles R. Farrar[2], M. ASCE

Abstract

Over the past 25 years, the use of vibrational parameters for detecting damage in a structure has received considerable attention from the civil, aerospace, and mechanical engineering communities. The general idea is that changes in the structure's physical properties, primarily stiffness, will alter the dynamic properties of the structure such as resonant frequencies and mode shapes. Properties such as the flexibility matrix, stiffness matrix, and mode shape curvature, which are obtained through manipulation of the modal parameters, have shown promise in localizing structural damage. In this paper, five techniques for damage assessment are demonstrated and compared using experimental and analytical data from a highway bridge.

Introduction

Because the Interstate 40 (I-40) bridges over the Rio Grande in Albuquerque, New Mexico were to be razed during the summer of 1993, the investigators from New Mexico State University (NMSU) were able to introduce simulated cracks into the structure in order to test various damage identification methods. To support this research effort, Los Alamos National Laboratory (LANL) performed experimental modal analyses, and developed experimentally verified numerical models of the bridge.

In this paper five damage identification methods that have been reported in the technical literature were applied to the experimental modal data measured on the I-40 Bridge. Subsequently, the same methods were applied to numerically generated modal data obtained from the finite element models previously mentioned. Once benchmarked against measured response of the undamaged and damaged bridge, the numerical models allowed damage at other locations and multiple damage scenarios to be studied.

Length limitations of this paper preclude a detailed discussion of the experimental modal analyses or the finite element modal analyses. The pertinent data obtained from both the experimental and analytical studies, required by all of the damage identification algorithms, were resonant frequencies and mode shapes for the damaged and undamaged bridge. For a more detailed summary of the tests performed

[1]Graduate Research Assistant, MS P946 Los Alamos National Laboratory, Los Alamos, NM 87545
[2]Staff Member, MS P946 Los Alamos National Laboratory, Los Alamos, NM 87545

on the I-40 Bridge and the results that were obtained, the reader is referred to Farrar, et al. (1994). A more detailed discussion of the finite element models can be found in Farrar, et al. (1995).

I-40 Bridge Geometry and Damage Scenarios

The existing I-40 Bridge over the Rio Grande consists of twin spans made up of a concrete deck supported by two welded-steel plate girders and three steel stringers. Loads from the stringers are transferred to the plate girders by floor beams. Cross-bracing is provided between the floor beams. Figure 1 shows an elevation view of the portion of the bridge that was tested. Connections that allow for thermal expansion (exp in Fig. 1) as well as connections that prevent longitudinal translation (pinned in Fig. 1) are located where the girder is supported by a concrete pier or abutment. The cross-section geometry of each bridge is shown in Fig. 2.

The damage that was introduced was intended to simulate fatigue cracking that has been observed in plate-girder bridges. Four levels of damage were introduced to the middle span of the north plate girder close to the seat supporting the floor beam at midspan. Damage was introduced by making various torch cuts in the web and flange of the girder. The first level of damage, designated E-1, consisted of a two-foot-long (61.0 cm) cut through the web approximately 3/8-in-wide (0.95-cm-wide) centered at midheight of the web. Next, this cut was continued to the bottom of the web, E-2 . During this cut the web, on either side of the cut, bent out of plane approximately 1 in.(2.54 cm). The flange was then cut halfway in from either side directly below cut in the web, E-3. Finally, the flange was cut completely through leaving the top 4 ft (122 cm) of the web and the top flange to carry the load at this location, E-4. Table I summarizes the additional cases that were analyzed with benchmarked finite element models. To reduce the run times, the concrete piers were removed from these models.

TABLE I

Summary of Finite Element Analysis Damage Cases

Damage Case	Location of Damage	Damage Description
A-1	midspan	lower one-third portion of web cut
A-2	midspan	lower one-third portion of web plus half of bottom flange cut
A-3	midspan	lower one-third portion of web plus entire bottom flange cut
A-4	one location: halfway between midspan and east support	lower one-third portion of web plus entire bottom flange cut
A-5	one location: one floor-beam-panel away from east support	lower one-third portion of web plus entire bottom flange cut
A-6	two locations: halfway between midspan and east support; one floor-beam-panel west of midspan	lower one-third portion of web plus entire bottom flange cut
A-7	one location: halfway between midspan and east support	lower one-third portion of web cut
A-8	one location: one floor-beam-panel away from east support	lower one-third portion of web cut

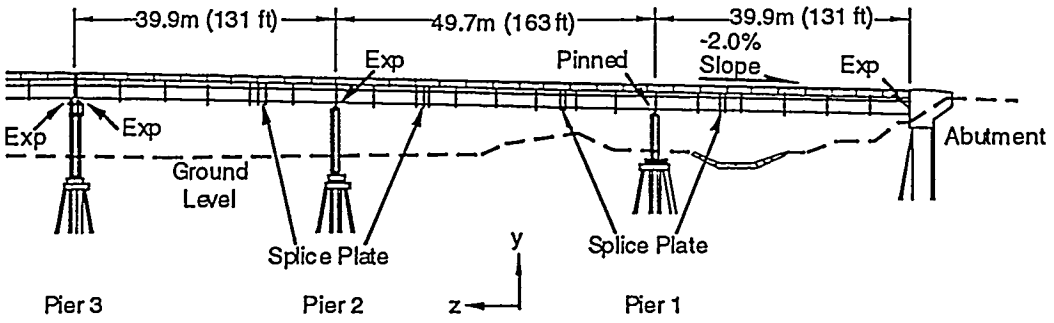

Figure 1. Elevation view of the portion of the eastbound bridge that was tested.

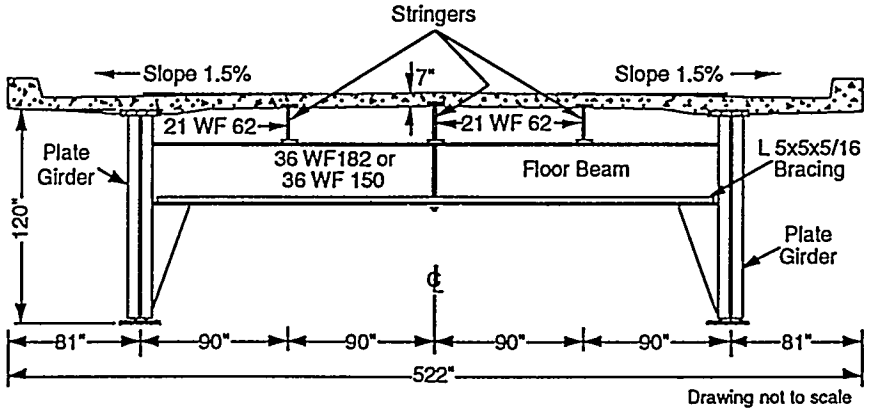

Figure 2. Typical cross-section geometry of the bridge.

Description of Damage Identification Methods

A very brief description of the damage identification methods that were used is given below. The reader is referred to the appropriate references for a more detailed discussion of these methods. A summary of their implementation for the study reported herein can be found in Farrar and Juaregui (1995).

Damage Index Method

The Damage Index Method was developed by Stubbs and Kim (1993) to localize damage in structures given their characteristic mode shapes before and after damage. For a structure that can be represented as a beam, a damage index, β, based on changes in curvature of the ith mode at location j is defined as

$$\beta_{ji} = \frac{\left(\int_a^b [\phi_i^{*}"(x)]^2 dx + \int_0^L [\phi_i^{*}"(x)]^2 dx\right)}{\left(\int_a^b [\phi_i"(x)]^2 dx + \int_0^L [\phi_i"(x)]^2 dx\right)} \cdot \frac{\int_0^L [\phi_i"(x)]^2 dx}{\int_0^L [\phi_i^{*}"(x)]^2 dx}, \quad (1)$$

where $\phi_i"(x)$ and $\phi_i^{*}"(x)$ are the second derivatives of the ith mode shape corresponding to the undamaged and damaged structures, respectively. L is the length of the beam. a and b are the limits of a segment of the beam where damage is being evaluated. Statistical methods are then used to examine changes in this index and associate these changes with possible damage locations.

Mode Shape Curvature Method

Pandey, Biswas, and Samman (1991) assume that structural damage only affects the stiffness matrix and not the mass matrix. Hence, for the undamaged and damaged condition the eigenvalue problems are given as

$$(K - \lambda_i M)\phi_i = 0, \text{ and } (K^* - \lambda_i^* M)\phi_i^* = 0, \text{ respectively,} \quad (2)$$

where K = the stiffness matrix, λ_i = the iih eigenvalue, M = the mass matrix, ϕ_i = the *i*th displacement eigenvector of the undamaged structure, and the asterisks signify quantities corresponding to the damaged structure. Curvature mode shapes for the beam in undamaged and damaged condition can then be estimated numerically from the displacement mode shapes with a central difference approximation or other means of differentiation. Larger differences in the pre- and post-damage curvature mode shapes are shown to be localized in the cracked region.

Change in Flexibility Method

For the undamaged and damaged structure, the flexibility matrix, F, is derived from the unit-mass-normalized modal data as follows

$$F = \Phi\Omega^{-1}\Phi^T = \sum_{i=1}^{n} \frac{1}{\omega_i^2}\phi_i\phi_i^T \text{ and } F^* = \Phi^*\Omega^{*-1}\Phi^{*T} = \sum_{i=1}^{n} \frac{1}{\omega_i^{*2}}\phi_i^*\phi_i^{*T}, \quad (3)$$

where Φ = the mode shape matrix = $[\phi_1, \phi_2, \ldots, \phi_n]$, ω_i = the ith modal frequency, Ω = the modal stiffness matrix = $\text{diag}(\omega_i^2)$, n = the number of degrees of freedom, and the asterisks signify properties of the damaged structure. From the pre- and post-damage flexibility matrices, a measure of the flexibility change caused by the damage can be obtained from the difference of the respective matrices. The column of the flexibility matrix corresponding to the largest change is indicative of the degree of freedom where the damage is located.

Change in Curvature Flexibility Shape Method

Recall that the coefficients of the ith column of the flexibility matrix represent the deflected shape assumed by the structure with a unit load applied at the ith degree of freedom. Zhang and Aktan (1995) state that the change in curvature of the uniform load flexibility can be used to determine the location of damage. The uniform load flexibility represents the deflected shape assumed by the structure when all degrees of freedom are loaded with a unit load. In terms of the uniform load flexibilities, the curvature change is evaluated as follows

$$\Delta = \left| \sum_{i=1}^{n} F_i^{*\prime\prime} - F_i^{\prime\prime} \right|, \quad (4)$$

where Δ and n represent the absolute curvature change and the number of degrees of freedom, respectively.

Change in Stiffness Method

Investigation of the eigenvalue problem before and after the onset of damage has revealed information for detecting damage as discussed by Zimmerman and Kaouk (1994). Letting ΔM_d and ΔK_d represent the perturbations to the original mass and stiffness matrices, the eigenvalue equation expands to

$$[\Omega^*(M - \Delta M_d) + (K - \Delta K_d)]\Phi^* = 0. \quad (5)$$

The damage vector, D, is then obtained by separating the terms containing the original matrices from those containing the perturbation matrices. Hence,

$$D = (\Omega^* M + K)\Phi^* = (\Omega^* \Delta M_d + \Delta K_d)\Phi^*. \quad (6)$$

To simplify the investigation, damage is usually considered to effect only the stiffness of a structure since substantial damage must occur to disrupt the mass. The damage vector then reduces to

$$D = \Delta K_d \Phi^*. \quad (7)$$

The stiffness matrices of the structure, before and after damage, can be derived from the modal parameters in a manner analogous to Eq. 3 and then used to compute ΔK_d.

Application of Damage Identification Methods to Numerical and Experimental Data

In this section, the linear damage identification methods are exercised using experimental and numerical modal data from the I-40 Bridge. The three sets of modal data (resonant frequencies and mode shapes) used are:

(1) SET1 - experimental modal data obtained via cross power spectra, refined sensor
(2) SET2 - experimental modal data obtained via polynomial curve fit of coarse sensor
(3) SET3 - numerical modal data obtained via cross power spectra, refined sensors

The coarse and refined sensor locations are shown in Figs. 3 and 4 respectively. When applying the damage identification algorithms to experimental or analytical data, values of the mode shape amplitudes at location between sensors were determined by fitting either a cubic spline or a cubic polynomial to the data from the measurement locations. In all cases, the span where damage was introduced was divided into 160 equal length elements. Table II summarizes the results of applying the Damage Index Method to the various sets of data and damage scenarios listed above. Similar tables were generated for the other damage identification algorithms.

Summary and Conclusions

Application of five linear damage identification routines using experimental and numerical modal data gathered from the I-40 Bridge has been reported. Extraction of the experimental modal data corresponding to the refined set of accelerometers and

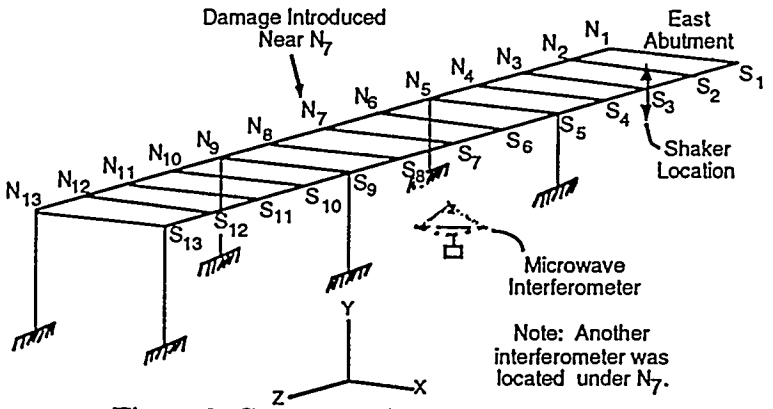

Figure 3. Coarse accelerometer locations.

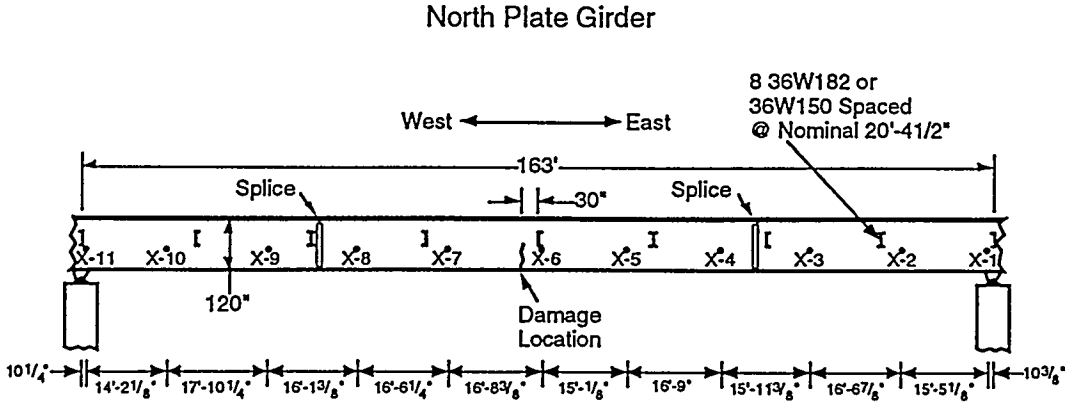

Figure 4. Refined accelerometer locations.

coarse set of accelerometers is discussed in Farrar, et. al. (1994). Numerical modal data was obtained using benchmarked finite element models of the I-40 Bridge.

Tables III through V summarize the results from applying the five damage detection algorithms to the experimental and numerical modal data. According to the tables, the Damage Index Method performed the best. The algorithm employed in this technique failed only for damage case A-7. For the remaining damage cases, the location of damage was either clearly identified or narrowed down to two locations. The Mode Shape Curvature Method also performed well, although not as well as the Damage Index Method. Only damage cases A-1 and A-2 went undetected using this technique. The Change in Flexibility Method appeared to have problems identifying damage for situations when damage was not severe. The Change in Curvature Flexibility Method performed satisfactorily using the experimental modal data from the refined set of accelerometers (SET1). The algorithms failed only for damage case E-1. The Change in Stiffness Method improved when applied to the modal data from the coarse set of accelerometers. Significant improvements were also shown when only the first two modes were used instead of all six as shown in Table V. Using the refined measurements, only the final damage case (E-4) was detected whereas all damage cases were detected from the SET2 modal data. When applied to the numerical data, the technique generated similar results as the Change in Flexibility Method (see Table V).

TABLE II

Comparison of Actual Damage Location with Damage Location Identified by Damage Index Method

Damage Case	Actual Damage Location	Damage Location Identified by Damage Index Method
E-1 through E-4 (SET1)	80	82
E-1 through E-4 (SET2)	80	106
A-1 through A-3 (SET3)	80	80
A-4(SET3)	40	40
A-5 (SET3)	20	20
A-6 * (SET3)	40, 100	40, 100
A-7 (SET3)	40	40
A-8 (SET3)	20	20

* Two locations of damage

TABLE III

Summary of Damage Detection Results using Experimental Modal Data from Refined Set of Accelerometers (SET1)

Damage Case	Damage Index Method	Mode Shape Curvature Method	Change in Flexibility Method	Change in Curvature Flexibility Method	Change in Stiffness Method
E-1	•	•••	○	○	○
E-2	•	••	○	•••	○
E-3	•	•	○	•	○
E-4	•	•	•	•	•

• Damage located, •• Damage narrowed down to two locations, •••Damage narrowed down to three locations, ○ Damage not located

TABLE IV

Summary of Damage Detection Results using Experimental Modal Data from Coarse Set of Accelerometers (SET2)

Damage Case	Damage Index Method	Mode Shape Curvature Method	Change in Flexibility Method	Change in Curvature Flexibility Method	Change in Stiffness Method
E-1	**	**	○	○	**
E-2	**	*	○	○	**
E-3	**	**	**	○	**
E-4	*	*	*	*	*

* Damage located, ** Damage located using only 2 modes; ○ Damage not located

Notable contributions of this work include: (1) the generation of numerical modal data in a manner which resembles the approach that would be followed given ambient vibration data; (2) the application of linear damage identification schemes based on changes in modal properties to these data; (3) direct comparison of the damage identification routines when applied to a common problem.

TABLE V

Summary of Damage Detection Results using Numerical Modal Data from Refined-Set of Monitored Responses (SET3)

Damage Case	Damage Index Method	Mode Shape Curvature Method	Change in Flexibility Method	Change in Curvature Flexibility Method	Change in Stiffness Method
A-1	••	◦	◦	◦	◦
A-2	••	◦	◦	◦	◦
A-3	•	•	◦	•	◦
A-4	•	•	•	•	•
A-5	•	•	•	•	•
A-6	•	•	•	•	•
A-7	◦	•	◦	◦	◦
A-8	••	•	◦	•	◦

• Damage located, •• Damage narrowed down to two locations, ••• Damage narrowed down to three locations, ◦ Damage not located

Acknowledgments

The authors would like to acknowledge the support of New Mexico State University in providing funding for this research effort.

References

Farrar, C. R., et al., (1994) "Dynamic Characterization and Damage Detection in the I-40 Bridge over the Rio Grande," Los Alamos National Lab report LA-12767-MS.

Farrar, C. R., et al., (1995) "Finite Element Analysis of the I-40 Bridge over the Rio Grande," Los Alamos National Lab report LA-12979-MS.

Farrar, C. R. and D. V. Jauregui (1995) "Damage Detection Algorithms Applied to Experimental and Analytical Modal Data from the I-40 Bridge," Los Alamos National Lab report (in print).

Kim, J.-T., and N. Stubbs (1993), *Assessment of the Relative Impact of Model Uncertainty on the Accuracy of Global Nondestructive Damage Detection in Structures,* report prepared for New Mexico State University.

Pandey, A. K., M. Biswas, and M. M. Samman (1991) "Damage Detection from Changes in Curvature Mode Shapes," *J. of Sound and Vibration*, **145**(2), 321-332.

Zhang, Z., and A. E. Aktan (1995) "The Damage Indices for the Constructed Facilities," *Proceedings of the 13th International Modal Analysis Conf.*, 2, 1520-1529.

Zimmerman, D. C. and M. Kaouk (1994) "Structural Damage Detection using a Minimum Rank Update Theory", *J.of Vibration and Acoustics*, **116**, 222-231.